Journal of Pathology
J Pathol February 2025; **265:** 172–183
Published online 29 November 2024 in Wiley Online Library
(wileyonlinelibrary.com) DOI: 10.1002/path.6375

ORIGINAL ARTICLE

Intravenous iron treatment fuels chronic kidney disease–induced arterial media calcification in rats

Astrid Van den Branden[1], Britt Opdebeeck[1], Saar Adriaensen[1], Pieter Evenepoel[2], Tom Vanden Berghe[1] and Anja Verhulst[1]*

[1] *Cell Death Signaling Lab, Department of Pharmaceutical, Biomedical and Veterinary Sciences, University of Antwerp, Antwerp, Belgium*
[2] *Nephrology and Renal Transplantation Research Group, Department of Microbiology, Immunology and Transplantation, KU Leuven, Leuven, Belgium*

**Correspondence to: A Verhulst, Cell Death Signaling Lab, University of Antwerp, Campus Drie Eiken, Universiteitsplein 1, B-2610 Wilrijk, Belgium.*
E-mail: anja.verhulst@uantwerpen.be

Abstract

Arterial media calcification is a severe cardiovascular complication commonly manifesting in patients with chronic kidney disease (CKD). Patients with CKD frequently undergo intravenous iron therapy to address iron deficiency. Iron is suggested to be sequestered in vascular cells, potentially leading to oxidative (lipid) stress and cell death, which are recognized as key contributors to arterial calcification. The objective of this study was to investigate the effect of intravenous iron administration on CKD-induced arterial media calcification. Therefore, adenine-induced CKD rats were treated intravenously with iron and checked for arterial iron deposition and calcification, as well as for ferritin and lipid peroxidation markers. Additionally, arterial sections from patients with CKD who were dialysis dependent were analyzed for these parameters. This study showed that intravenous iron administration in CKD rats led to arterial iron deposition and a lipid peroxidation signature. CKD-induced arterial calcification was increased upon iron treatment and correlated with arterial iron accumulation and lipid peroxidation markers. Patients with CKD who were dialysis dependent showed arterial iron accumulation and elevated lipid peroxidation, but a direct correlation with arterial calcification was lacking. Taken together, iron treatment is suggested as a potential contributor to the calcification process, instead of being a predominant factor, thereby emphasizing the complexity of arterial calcification as a multifactorial disease.

Keywords: arterial calcification; chronic kidney disease; hepcidin; iron; lipid peroxidation

Received 22 April 2024; Revised 9 September 2024; Accepted 24 October 2024

Conflict of interest statement: TVB holds patents related to ferroptosis inhibitors (US9862678, WO2016075330, EP3218357, WO2019154795). PE has received grants and consulting fees from Vifor CSL. No other conflicts of interest were declared.

Introduction

Arterial media calcification is a common complication in patients with chronic kidney disease (CKD) for which no effective therapy is available [1]. It is characterized by the pathological accumulation of calcium phosphate crystals in the medial layer of the vessel wall. Arterial calcification places patients at high risk of developing serious cardiovascular complications and mortality [2,3], imposing a large burden on both healthcare and the economy [4]. Of note, the risk of dying of cardiovascular disease in patients with early-stage CKD surpasses the risk of progressing to end-stage renal disease [5].

Aside from arterial calcification, many patients with CKD have absolute and functional iron deficiency [6]. Absolute iron deficiency results from malnutrition or gastrointestinal bleeding, blood requirements for laboratory tests and blood retention during hemodialysis therapy [6,7]. Functional iron deficiency is characterized by low circulating iron concentrations despite adequate body iron stores. The primary culprit behind this deficiency is increased hepcidin levels. Hepcidin acts as a key regulator of iron homeostasis by controlling intestinal iron absorption by enterocytes and iron release from macrophages and hepatocytes [8,9]. Hepcidin achieves this via degradation of ferroportin, a transmembrane protein responsible for cellular iron excretion [10], eventually leading to cellular iron sequestration [11]. Circulating hepcidin levels in patients with CKD are increased because of impaired renal clearance and elevated hepatic synthesis, triggered by inflammation and alterations in iron status [12,13].

To alleviate iron deficiency in patients with CKD, iron supplementation is commonly used as a key component of their treatment regimen. Intravenous (i.v.) iron is preferred over the oral route due to limited effectiveness of oral administration (caused by hepcidin-induced

blockade of gastrointestinal absorption [14]) and the ease of using the existing vascular access in patients receiving dialysis [15]. However, since ferroportin expression is also present in arterial cells [16–18], i.v. iron can potentially be sequestered in arterial cells due to increased serum hepcidin levels. In this context, it is interesting to mention that a direct calcification aggravating effect of iron was observed *in vitro* in calcifying vascular smooth muscle cells (VSMCs) [19].

Cellular iron excess can readily elevate the risk of oxidative stress. Iron promotes the generation of reactive hydroxyl radicals via the Fenton reaction [20]. These radicals are capable of causing oxidative stress, a recognized contributor to the development of arterial calcification [21,22], and can also react with polyunsaturated fatty acid containing phospholipids in the cell membrane. This leads to the accumulation of toxic lipid hydroperoxides and membrane damage (i.e. lipid peroxidation), ultimately triggering ferroptotic cell death [23–25]. A critical defense mechanism against lipid peroxidation/ferroptosis is mediated by glutathione peroxidase 4 (Gpx4), an enzyme that reduces toxic lipid hydroperoxides to lipid alcohols [26]. The role of Gpx4 is crucial because its impairment can lead to excessive lipid peroxidation and increased ferroptotic cell death, which goes along with the formation of harmful by-products such as 4-hydroxy-2-nonenal (4HNE). 4HNE is a highly reactive aldehyde that not only exacerbates cellular oxidative damage but also serves as a specific marker of lipid peroxidation [27]. Interestingly, an important role for cell death in arterial calcification development has been described in the past, where dead VSMCs serve as an excellent nidus for calcium phosphate crystal deposition [28,29].

Although lipid peroxidation/ferroptosis has been implicated in several cardiovascular diseases [30,31], its role in the development of arterial media calcification remains unclear. Recent publications have illustrated a contribution of lipid peroxidation/ferroptosis to arterial calcification, while inhibition of ferroptosis attenuated arterial calcification [32–34]. Considering this, investigating the effect of i.v. iron treatment on arterial calcification in a CKD context is warranted. Therefore, this study investigated whether i.v. iron sucrose administration induces arterial iron accumulation, thereby altering the development of arterial media calcification in a rat model of adenine-induced CKD, with a special focus on lipid peroxidation/ferroptosis as underlying mechanisms. Arterial tissue of patients receiving dialysis was analyzed to provide a more comprehensive insight into this hypothesis.

Materials and methods

Animals

Experimental procedures were approved by the Antwerp University Ethics Committee (ECD code 2021-73). Fifty male Wistar Han rats (225–250 g; Charles River, Beerse, Belgium) were housed at the Antwerp University animal facility under constant environmental conditions (12/12 h light/dark cycles) with *ad libitum* access to food and water. To induce stable CKD, animals were exposed to adenine via oral gavage for nine consecutive days (600 mg/kg/day; Acros Organics, Geel, Belgium) and fed a phosphate-enriched diet for the entire study (1.2% Pi-1.06% Ca; SSNIFF Spezialdiäten, Soest, Germany). CKD rats were randomly assigned to receive (i) vehicle (0.9% NaCl; $n = 11$), (ii) 3 mg/kg/dose iron ($n = 10$) or (iii) 10 mg/kg/dose iron ($n = 11$). Iron was administered as iron sucrose (Venofer; CSL Vifor, Glattbrugg, Switzerland). The 3 mg/kg dose closely mirrors the therapeutic dosage of iron sucrose administered to patients receiving hemodialysis (100–200 mg/dialysis session for adult patients at an average 70 kg), while the 10 mg/kg dose was included in the study as a supratherapeutic dose to investigate dose dependency. Vehicle and iron were administered i.v. via the tail vein three times a week starting after CKD induction for a 4-week treatment period. Control rats with normal renal function, treated with vehicle or the (supra)therapeutic iron dose, were also included ($n = 6$ each).

After the 4-week treatment with vehicle/iron, rats were sacrificed by exsanguination after anesthesia with intraperitoneal administration of 80 mg/kg ketamine (Ketalar; Pfizer, New York, NY, USA) and 10 mg/kg xylazine (Rompun; Dechra Pharmaceuticals, Northwich, UK).

Serum analyses

Blood samples were collected via the tail vein at intermediate time points and at sacrifice from the retro-orbital plexus. To assess renal function, serum phosphorus and creatinine levels were quantified. Phosphorus levels were determined by the molybdate method using the Ecoline S Phosphate kit (Diasys Diagnostic Systems, Holzheim, Germany). Creatinine levels were measured according to the Jaffé method. Serum hepcidin levels were measured using a commercially available ELISA kit (Cusabio, Houston, TX, USA). Serum iron concentrations were determined via electrothermal atomic absorption spectroscopy (ETAAS; PerkinElmer, Shelton, CT, USA). For sample preparation, 0.3 M hydrochloric acid was added, and the samples were incubated for 1 h at room temperature. Subsequently, a 20% solution of trichloroacetic acid was introduced into the samples. The supernatant obtained after centrifugation was used to determine the serum iron levels.

Arterial iron accumulation

Iron levels were quantified via ETAAS (PerkinElmer) in two parts of the thoracic aorta. The thoracic aorta was harvested at sacrifice, rinsed with 0.9% NaCl, stripped from adherent tissue and subdivided as follows: (1) the aortic arch, comprising aortic tissue above the heart (including the thoracic ascending aorta and a part of the thoracic descending aorta); and (2) the thoracic aorta, defined as the segment of the thoracic descending aorta extending from below the aortic arch to the diaphragm. Tissues were wet-weighed on a precision balance and

digested in 65% nitric acid at 60 C overnight, after which the iron levels were determined.

The diaminobenzidine (DAB)-enhanced Turnbull blue staining method (Hametner *et al* [35]) was used to detect iron in paraffin-embedded thoracic aorta sections. These were incubated for 90 min in 2% ammonium sulfide and immersed in 10% potassium ferricyanide/0.5% hydrochloric acid for 15 min, followed by several washes with distilled water. Next, endogenous peroxidase activity was blocked with 0.01 M sodium azide and 0.3% hydrogen peroxide, followed by a washing step with 0.1 M phosphate buffer. Finally, iron staining was amplified with DAB (ImmPACT DAB substrate kit, SK-4105, Vector Laboratories, Newark, CA, USA) to visualize iron as brown dots. Sections were counterstained with hematoxylin. Images were taken using a Leica DMR microscope (Leica Microsystems, Wetzlar, Germany). Fiji image analysis software was used to assess the percentage iron-positive area relative to the total area. Due to the inherent hardness of calcified tissue, fracturing is an unavoidable limitation during tissue sectioning. These tissue fractures were excluded from total tissue area during quantitative analysis. Additionally, these fractures were also observed in other staining procedures described later in this manuscript and were similarly excluded from analysis.

Evaluation of arterial calcification

Arterial calcification degree was evaluated by measurement of the calcium content in the aortic arch and thoracic aorta, and quantifying the percentage calcified area on Von Kossa-stained sections. Calcium content was determined in the same tissue digestion liquid as used for iron measurement by flame atomic absorption spectrometry (PerkinElmer). The samples were first diluted with 0.1% lanthanum nitrate to eliminate chemical interference.

To visualize/quantify calcification in the arterial wall, thoracic aorta sections were stained with Von Kossa and counterstained with hematoxylin/eosin. Von Kossa positivity is seen as black deposits. Using Fiji image analysis software, the percentage calcified area was defined, calculated as the ratio of Von Kossa-positive area to the total tissue area. In addition to Von Kossa staining, which identifies phosphate, Alizarin red staining was performed, followed by fast green counterstaining, to visualize calcium deposits.

Immunohistochemical staining of arterial tissue

Thoracic aorta sections were immunohistochemically stained for ferritin, Gpx4 and 4HNE, and hematoxylin counterstained. Sections were decalcified with 1% acetic acid and heat-mediated epitope retrieval was performed using a citrate-based antigen unmasking solution (H-3300, Vector Laboratories). Blocking of non-specific binding sites with normal goat serum (P30-1001, Pan Biotech, Aidenbach, Germany) for 20 min (20% in TBST) was followed by overnight incubation with primary antibodies for ferritin (10727-1-AP, 1/1000, Proteintech Group, Rosemont, IL, USA), Gpx4 (ab125066, 1/500, Abcam, Cambridge, UK) and 4HNE (ab46545, 1/500, Abcam). Endogenous peroxidase activity was suppressed via a 3% hydrogen peroxide solution and biotinylated goat-anti rabbit (PK-4001, Vector Laboratories) was used as secondary antibody. Subsequently, avidin/biotinylated peroxidase complex (VECTASTAIN ABC kit, Vector Laboratories) was added as signal amplifier using DAB (Vector Laboratories) as substrate, producing a brown color. Ferritin, Gpx4 and 4HNE positivity (% positive area) relative to the total tissue area was quantified. Negative controls (omission of primary antibody) were performed concurrently.

Staining of human arterial tissue

Part of the epigastric artery was harvested from patients with end-stage kidney disease at the time of kidney transplantation surgery ($n = 40$). Informed consent was obtained and the procedure was approved by the ethical committee of the University Hospital Leuven. Iron treatment was in accordance with the international KDIGO guidelines. Arterial sections were stained with (1) Von Kossa, (2) DAB-enhanced Turnbull, and (3) immunohistochemical staining of ferritin (10727-1-AP, 1/2000, Proteintech), Gpx4 (ab125066, 1/500, Abcam) and 4HNE (ab46545, 1/500, Abcam). Staining intensities were subjected to a scoring system ranging from − to ++++: − = no staining, + = weak staining, ++ = mild staining, +++ = moderate staining and ++++ = strong staining. The scoring of the stained samples was performed independently by two individuals.

Statistical analysis

Statistical comparisons were performed by non-parametric testing using GraphPad Prism software (Graphpad Software, version 10.1.2, San Diego, CA, USA). Statistical differences between multiple groups were assessed by the Kruskal–Wallis test, followed by Dunn's multiple comparison test when significant. The comparison between two groups (CKD group versus its corresponding non-CKD group) was performed using a two-tailed Mann–Whitney *U*-test. To investigate the relationship between numerical variables, a Spearman ρ univariate correlation analysis was performed and Fisher's exact test for categorical variables. Data in the text are presented as median [interquartile range (IQR)]. Results were considered significant when the adjusted p value was ≤0.05.

Results

Induction of stable, severe CKD

Stable and severe CKD was induced in all CKD groups after adenine administration, evidenced by significantly elevated serum creatinine (Table 1) and phosphorus (Table 2) levels compared with non-CKD vehicle rats. Importantly, no significant differences were observed

Table 1. Serum creatinine levels.

Group	Creatinine (mg/dl)		
	Start i.v.	2-week treatment	Sacrifice
Non-CKD vehicle	1.18 (0.14)	1.60 (0.31)	1.51 (0.71)
Non-CKD 3 mg/kg iron	1.21 (0.72)	1.45 (0.61)	1.39 (0.27)
Non-CKD 10 mg/kg iron	1.08 (0.41)	1.45 (0.46)	1.20 (0.17)
CKD vehicle	6.06 (2.98)***	5.30 (1.70)***	6.05 (4.53)***
CKD 3 mg/kg iron	6.94 (2.81)***	5.77 (3.26)**	6.42 (1.67)**
CKD 10 mg/kg iron	7.03 (2.57)***	5.17 (1.31)***	5.91 (3.51)**

Data are presented as median (interquartile range). Start i.v. = after the induction of CKD and prior to the start of i.v. treatment. Two-tailed Mann–Whitney *U*-tests (each CKD group versus non-CKD vehicle) at the same time point. Significance versus non-CKD vehicle at the same time point: **$p < 0.01$; ***$p < 0.001$.
CKD, chronic kidney disease.

Table 2. Serum phosphorus levels.

Group	Phosphorus (mg/dl)		
	Start i.v.	2-week treatment	Sacrifice
Non-CKD vehicle	10.90 (5.23)	9.70 (1.65)	10.29 (3.55)
Non-CKD 3 mg/kg iron	8.12 (3.85)	9.36 (2.63)	8.36 (3.46)
Non-CKD 10 mg/kg iron	8.61 (3.61)	7.96 (2.94)	7.21 (3.03)
CKD vehicle	21.62 (6.64)***	27.38 (11.99)***	26.05 (18.34)***
CKD 3 mg/kg iron	23.56 (4.14)***	24.14 (7.80)**	20.49 (6.64)**
CKD 10 mg/kg iron	24.75 (3.48)***	20.72 (12.03)***	17.20 (12.16)**

Data are presented as median (interquartile range). Start i.v. = after the induction of CKD and prior to the start of i.v. treatment. Two-tailed Mann–Whitney *U*-tests (each CKD group versus non-CKD vehicle) at the same time point. Significance versus non-CKD vehicle at the same time point: **$p < 0.01$; ***$p < 0.001$.
CKD, chronic kidney disease.

between creatinine and phosphate levels of the different CKD groups.

CKD groups experienced mortality before the planned sacrifice: two rats in the vehicle-treated group (two in week 2), three rats in the therapeutic (two in week 2, one in week 3) and five rats in the supratherapeutic (one in week 1, two in week 2, two in week 3) iron-treated groups. Animals that did not reach the planned sacrifice point were also included for analysis.

Iron accumulates in arteries of iron-treated animals with chronic kidney disease and correlates with arterial ferritin expression

Iron treatment led to increased arterial iron levels in CKD rats, including both the thoracic aorta and aortic arch (Figure 1A,B). For the supratherapeutic iron-treated CKD group, this increase was significant in the thoracic aorta ($p = 0.025$) in comparison to vehicle-treated CKD animals. The presence of arterial iron depositions in iron-treated CKD rats was visually confirmed on Turnbull-stained arterial sections (Figure 1C,D). Iron did not accumulate in rats with normal renal function, regardless of their treatment (supplementary material, Figure S1A).

Arterial sections were also stained to detect ferritin expression (Figure 1E). In the iron-treated CKD groups, the arterial ferritin levels were significantly higher than in vehicle-treated CKD animals (therapeutic iron: $p = 0.020$, supratherapeutic iron: $p < 0.0001$) (Figure 1F), whereas no arterial ferritin expression was present in rats with normal renal function (supplementary material, Figure S1B). Moreover, arterial ferritin expression shows a strong positive correlation with iron deposition in the CKD iron-treated groups ($\rho = 0.69$, $p = 0.0005$) (Figure 1G). In summary, these data show that iron treatment in CKD rats leads to arterial iron accumulation, which correlates with arterial ferritin expression.

Arterial iron accumulation correlates with calcium deposition in iron-treated animals with chronic kidney disease

Adenine-induced CKD triggered the development of arterial media calcification as evidenced by significantly increased calcium content in the thoracic aorta ($p = 0.020$) and aortic arch ($p = 0.0031$) of vehicle-treated CKD rats versus non-CKD vehicle-treated rats [thoracic: non-CKD = 0.29 (IQR 0.17) mg/g tissue, CKD = 0.43 (3.16) mg/g tissue; arch: non-CKD = 0.25 (0.23) mg/g tissue, CKD = 1.02 (23.63) mg/g tissue]. Interestingly, administration of the supratherapeutic iron dose to CKD rats significantly aggravated the arterial calcium content (thoracic: $p = 0.0097$; arch: $p = 0.025$) compared with vehicle-treated CKD rats (Figure 2A,B). Microscopic confirmation of crystal deposition in the medial arterial layer of CKD animals was obtained after Von Kossa staining (detecting phosphate) of tissue sections (Figure 2C,D). The calcium-detecting Alizarin red staining method revealed equal patterns of crystal deposition, but appeared to be less sensitive compared with the Von Kossa staining as the smallest calcified spots could only be detected by the Von Kossa method (supplementary material, Figure S2). Consequently, Von Kossa-stained sections were selected for quantification. A significantly increased percentage of calcified tissue area was found in supratherapeutic iron-treated CKD rats

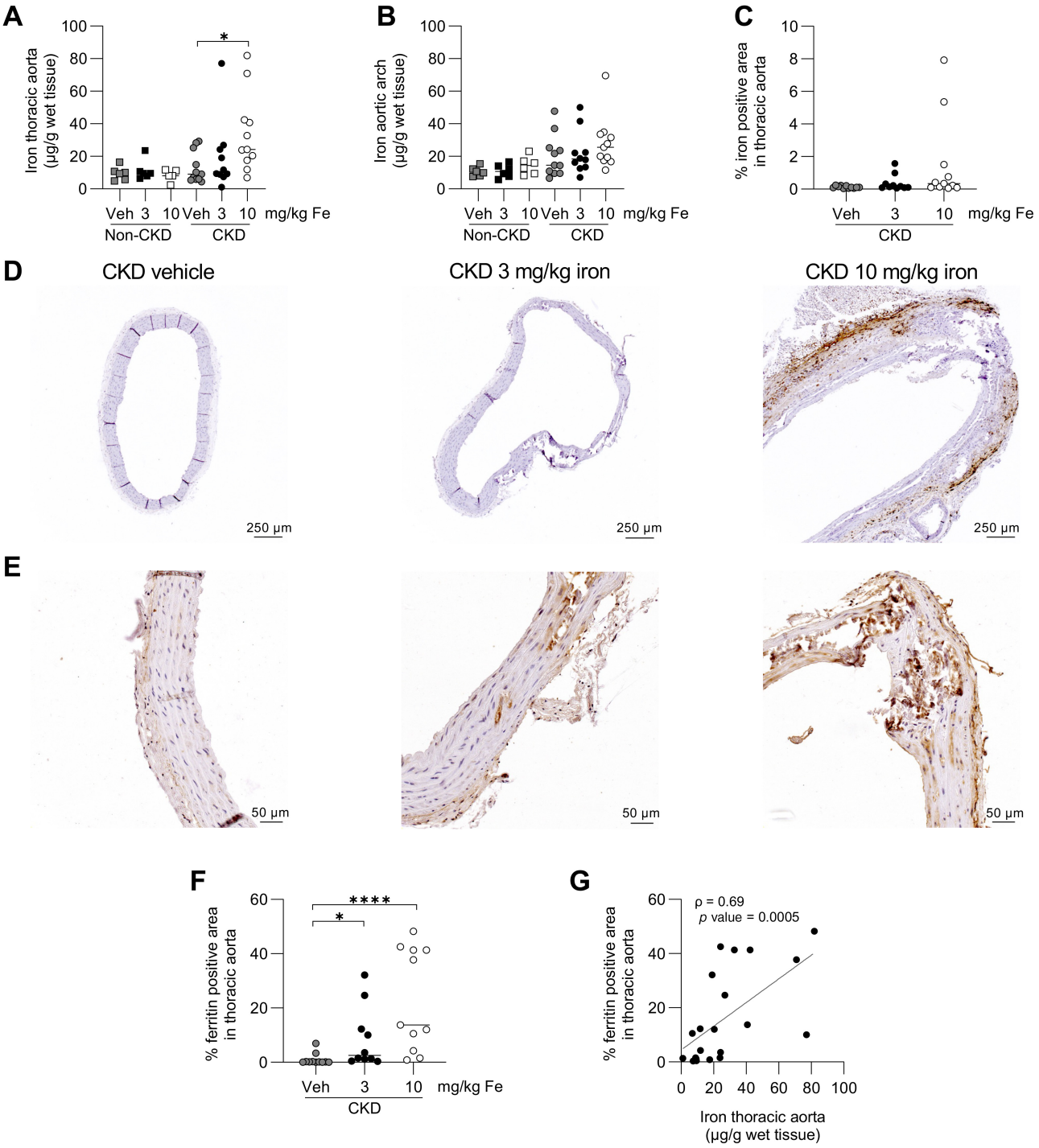

Figure 1. Iron levels in (A) the thoracic aorta and (B) the aortic arch. (C) Quantification of total iron positive area (%) in thoracic aortic sections of CKD animals. Representative images of (D) diaminobenzidine-enhanced Turnbull iron staining and (E) ferritin staining for CKD vehicle, 3 mg/kg iron and 10 mg/kg iron treated rats. Iron and ferritin positivity are shown as brown depositions. (F) Quantification of aortic ferritin positive area (%) in CKD animals. Data are presented as individual values (dots) and median (line). Kruskal–Wallis with Dunn's multiple correction for the CKD groups versus CKD vehicle group. Significance versus CKD vehicle group: *$p < 0.05$, ****$p < 0.0001$. (G) Correlation between ferritin positivity (%) and thoracic aortic iron levels in CKD iron-treated rats. Spearman's ρ correlation analysis and simple linear regression were performed. ρ = Spearman's rank correlation coefficient. CKD, chronic kidney disease; Fe, iron; veh, vehicle.

($p = 0.0025$) compared with vehicle-treated CKD rats. Total calcium levels and percentage calcified area of therapeutic dose iron-treated CKD rats were not significantly different from CKD vehicle animals. Non-CKD animals, either treated with vehicle or iron, did not develop arterial calcification (supplementary material, Figure S1C).

Furthermore, there is a strong positive relationship between arterial calcification and iron deposition, as evidenced by significant correlations between calcium and iron levels in the thoracic aorta ($\rho = 0.74$, $p = 0.0001$) and aortic arch ($\rho = 0.84$, $p < 0.0001$) of iron-treated CKD animals (Figure 2E,F, upper part).

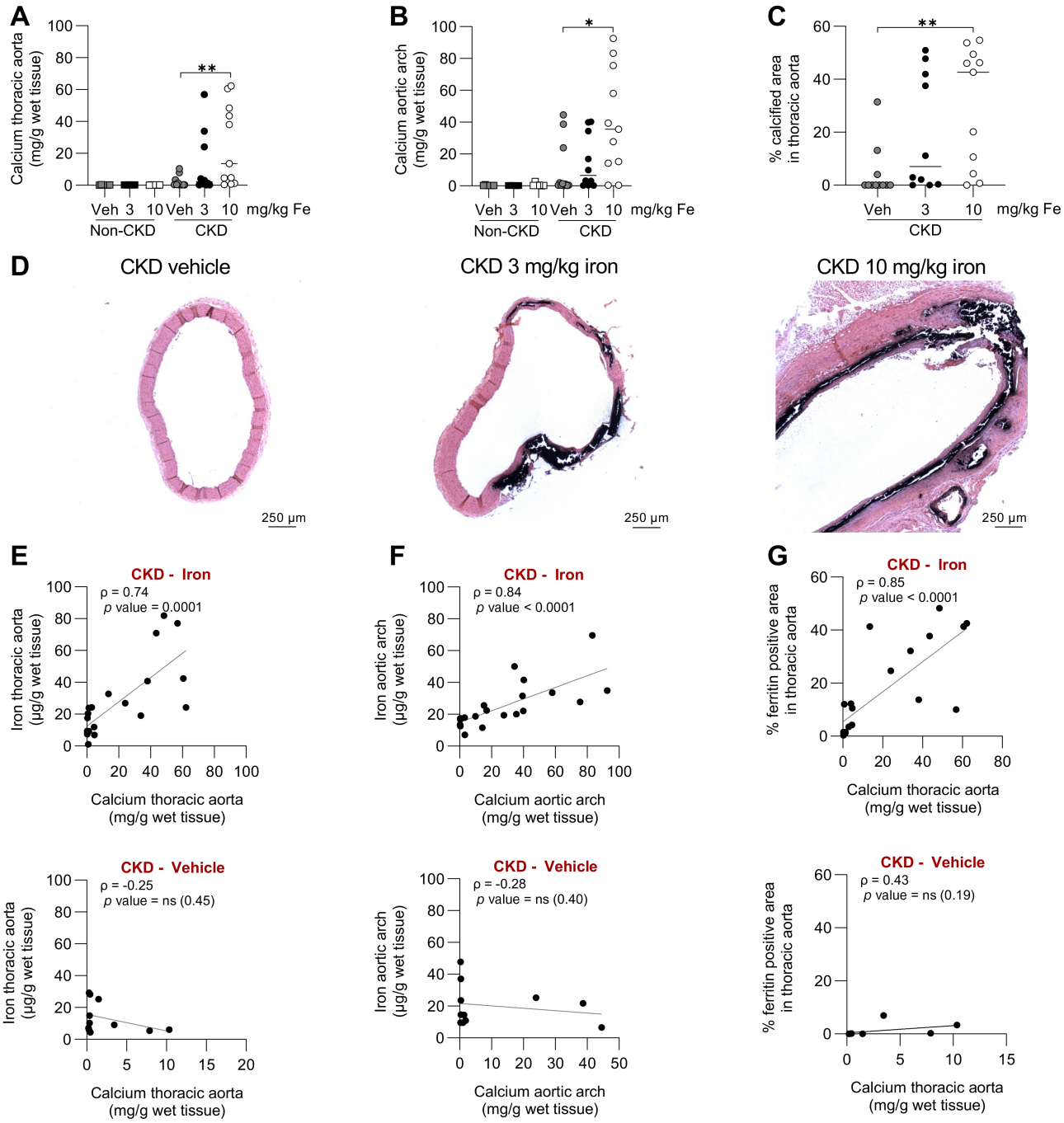

Figure 2. Calcium levels in (A) the thoracic aorta and (B) the aortic arch. (C) Quantification of Von Kossa positive area (% calcified area in the aorta) in thoracic aortic sections of CKD animals. (D) Representative images of Von Kossa-stained aortic sections for CKD vehicle, 3 mg/kg iron and 10 mg/kg iron treated rats. Von Kossa positivity is seen as black deposits. Data are presented as individual values (dots) and median (line). Kruskal–Wallis with Dunn's multiple correction for the CKD groups versus CKD vehicle group. Significance versus CKD vehicle group: $^{*}p < 0.05$, $^{**}p < 0.01$. Relationship between calcium and iron levels in both the (E) thoracic aorta and (F) aortic arch in CKD animals treated with iron (upper part) and vehicle (lower part). (G) Correlation between calcium accumulation (thoracic aorta) and aortic ferritin expression in iron-treated and vehicle-treated CKD rats. Spearman's ρ correlation analysis and simple linear regression were performed. ρ = Spearman's rank correlation coefficient. CKD, chronic kidney disease; veh, vehicle; Fe, iron.

No significant correlations were found between arterial calcification and iron accumulation in the CKD vehicle-treated group (Figure 2E,F, lower part). Arterial calcification also significantly correlated with arterial ferritin expression in iron-treated CKD animals ($\rho = 0.85$, $p < 0.0001$), but not in the CKD vehicle group (Figure 2G). Altogether, iron treatment of CKD rats aggravates arterial calcification, which also shows a significant correlation with arterial iron deposition and ferritin expression.

Iron dyshomeostasis and ferroptosis signature as reaction on iron treatment

Serum iron concentrations were significantly increased in non-CKD animals after treatment with the supratherapeutic

iron dose ($p = 0.0024$) compared with vehicle-treated non-CKD animals [vehicle = 1,034 (114.2) µg/l, supratherapeutic iron = 1,566 (632.0) µg/l], whereas this increase was not present within the CKD groups. Remarkably, serum iron levels were significantly decreased in the iron-treated CKD animals (therapeutic iron: $p = 0.0046$, supratherapeutic iron: $p = 0.0031$), as well as the vehicle CKD group ($p = 0.0048$) in comparison to their corresponding non-CKD group (Figure 3A). Serum hepcidin levels were significantly elevated in all CKD groups compared with their respective non-CKD group (vehicle: $p = 0.0002$, therapeutic iron: $p = 0.0002$, supratherapeutic iron: $p = 0.0002$) (Figure 3B).

Immunohistochemical staining of arterial sections was performed to visualize and quantify the presence of Gpx4 (Figure 4A,B) and 4HNE (Figure 4C,D), respectively a critical suppressor and marker of lipid peroxidation/ferroptosis. No Gpx4 or 4HNE could be detected in the arteries of non-CKD rats (supplementary material, Figure S1D,E). Contrastingly, CKD vehicle-treated animals showed significantly elevated levels of Gpx4 ($p = 0.0046$) and 4HNE ($p = 0.0048$) compared with non-CKD vehicle-treated rats [Gpx4: non-CKD = 0.003% (0.033%), CKD = 0.100% (0.324%); 4HNE: non-CKD = 0.055% (0.104%), CKD = 1.124% (2.996%)]. In addition, iron administration in CKD rats increased Gpx4 and 4HNE positivity compared with vehicle-treated CKD rats, which was significant for Gpx4 in the animals treated with the supratherapeutic iron dose ($p = 0.049$).

Remarkably, the relationship between Gpx4 expression ($\rho = 0.85$, $p < 0.0001$) and 4HNE presence ($\rho = 0.76$, $p < 0.0001$) versus arterial calcification (on Von Kossa-stained sections) was strongly positive in iron-treated CKD animals (Figure 4E,F, left column). No significant correlations were observed in the CKD vehicle-treated group (Figure 4E,F, right column). In addition, Gpx4 expression correlated with arterial ferritin expression ($\rho = 0.79$, $p < 0.0001$) and iron deposition on iron-stained aortic sections ($\rho = 0.74$, $p = 0.0001$) in iron-treated CKD animals. These findings highlight the effect of iron supplementation on altering the iron homeostasis and increasing biomarkers of lipid peroxidation/ferroptosis.

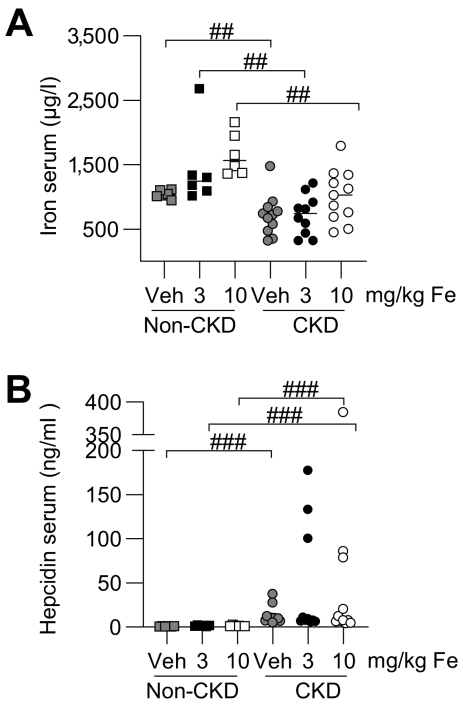

Figure 3. Serum (A) iron and (B) hepcidin levels. Data are presented as individual values (dots) and median (line). Serum iron and hepcidin levels were measured at the latest timepoint at which blood was collected from each individual animal, including animals that died before planned sacrifice. Two-tailed Mann–Whitney *U*-tests between CKD groups and their corresponding non-CKD group. Significance versus corresponding non-CKD group: $^{\#\#}p < 0.01$, $^{\#\#\#}p < 0.001$. CKD, chronic kidney disease; Fe, iron; veh, vehicle.

Association of lipid peroxidation markers and ferritin expression in calcified human arterial tissue, though not with arterial calcification

Arterial calcification was present among all samples, albeit with varying degrees ranging from weak to strong staining (Figure 5A). Turnbull staining showed no detectable iron accumulation in any of the samples (images not shown). Across all samples, varying levels of ferritin, Gpx4 and 4HNE were observed (Figure 5B–D and supplementary material, Figure S3). Ferritin expression and lipid peroxidation markers were not associated with calcification (Figure 5E–G), though ferritin showed a significant association with the presence of Gpx4 ($p = 0.0089$) (Figure 5H), not 4HNE (Figure 5I). The consistent results of the second independent observer can be found in supplementary material, Figure S4 (no average score of the two analyses could be calculated due to the categorical nature of the classification). Thus, human calcified arteries show a lipid peroxidation signature associated with ferritin, but not with arterial calcification.

Discussion

Conflicting clinical data have been published about iron supplementation and cardiovascular-related events in patients receiving hemodialysis [36–38]. Also, conflicting results have been reported in animal studies about the association between iron overload and arterial calcification [39,40]. To shine light on the potential impact of i.v. iron administration on the progression of arterial media calcification, the effect of iron sucrose administration was evaluated in an experimental rat model of adenine-induced CKD.

Iron accumulated in the medial layer of the vessel wall in the CKD groups upon iron treatment. Moreover, iron exposure aggravated the degree of arterial calcification. This is further supported by the strong positive correlation between arterial iron and calcium levels in iron-treated CKD rats, suggesting direct involvement of iron accumulation in arterial calcification. Also important

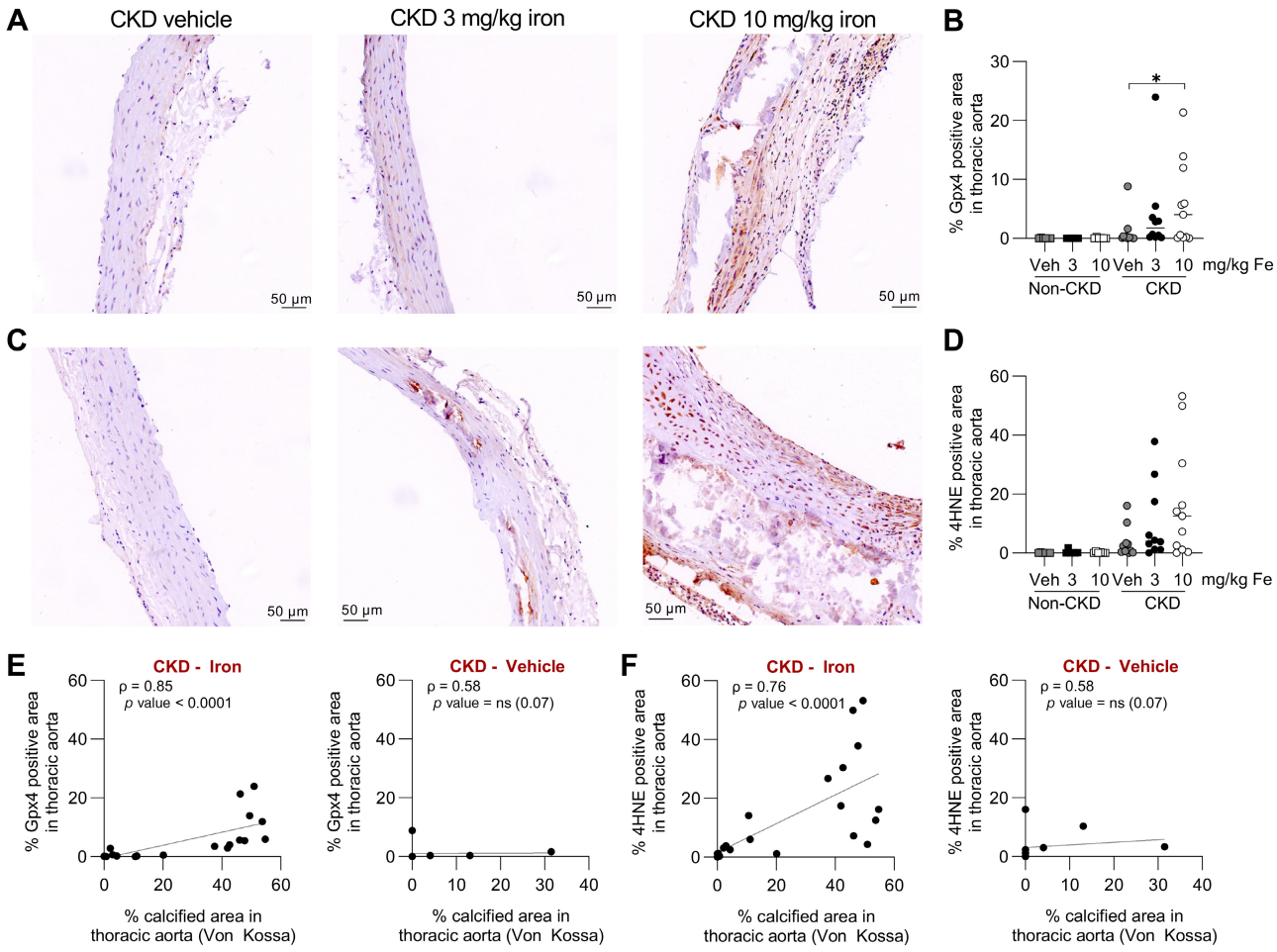

Figure 4. Representative images and quantification of positive area (%) of Gpx4 (A, B) and 4HNE (C, D) of thoracic aortic sections for CKD vehicle, 3 mg/kg iron and 10 mg/kg iron treated CKD rats. Gpx4 and 4HNE positivity is shown as brown deposits. Data are presented as individual values (dots) and median (line). Kruskal–Wallis with Dunn's multiple correction for the CKD groups versus CKD vehicle group. Significance versus CKD vehicle group: $^*p < 0.05$. Correlation between (E) Gpx4 expression and (F) 4HNE presence versus % calcified area (on Von Kossa-stained aortic sections) in iron (left graph) and vehicle treated CKD rats (right graph). Spearman's ρ correlation analysis and simple linear regression were performed. ρ = Spearman's rank correlation coefficient. 4HNE, 4-hydroxy-2-nonenal; CKD, chronic kidney disease; Fe, iron, Gpx4, glutathione peroxidase 4; veh, vehicle.

to mention, however, is that a subset of iron-exposed CKD rats did not manifest significant arterial calcifications. This divergence could be attributed to their potential capacity to hinder iron accumulation, as indicated by the positive arterial iron–calcium correlation.

Although concerns have been raised in the literature regarding potential nephrotoxicity of parenteral iron administration [41,42], iron exposure did not worsen renal function in CKD animals, aligning with the findings of Nuhu *et al* [43]. This suggests that iron treatment triggers the progression of arterial media calcification via direct deleterious effects on the vessel wall.

Serum iron levels were significantly decreased in the CKD groups compared with their respective non-CKD groups, probably due to markedly elevated serum hepcidin levels measured in the CKD groups. Hepcidin is a circulating hormone, facilitating intracellular iron accumulation. In this way, during CKD, iron can get trapped in cells, including vascular cells, as suggested by the increased arterial iron levels observed in this study. Moreover, the intracellular iron storage protein ferritin was highly expressed in arterial tissue of iron-treated CKD rats and its expression significantly correlated with the level of arterial iron accumulation and calcification. Remarkably, iron/ferritin accumulated in close proximity to spots of calcification. Interestingly, the co-localization of iron/ferritin and calcium has been reported earlier in diseased human cardiovascular tissue [44,45].

Intracellular iron excess may have triggered peroxidative lipid stress in arteries of iron-treated CKD animals. This is in line with (1) clinical data showing that iron therapy in patients with CKD increased oxidative stress and lipid peroxidation [46,47]; and (2) the fact that Gpx4 expression and 4HNE presence were also (significantly) increased in animals treated with the highest iron dose. Furthermore, the strong positive correlation between arterial calcification and 4HNE presence/Gpx4 expression, as found in the present study, is of particular interest. 4HNE is a toxic lipid peroxidation product, indicative of increased cellular damage due to oxidative stress and lipid peroxidation. On the other hand, Gpx4 plays a crucial role in reducing

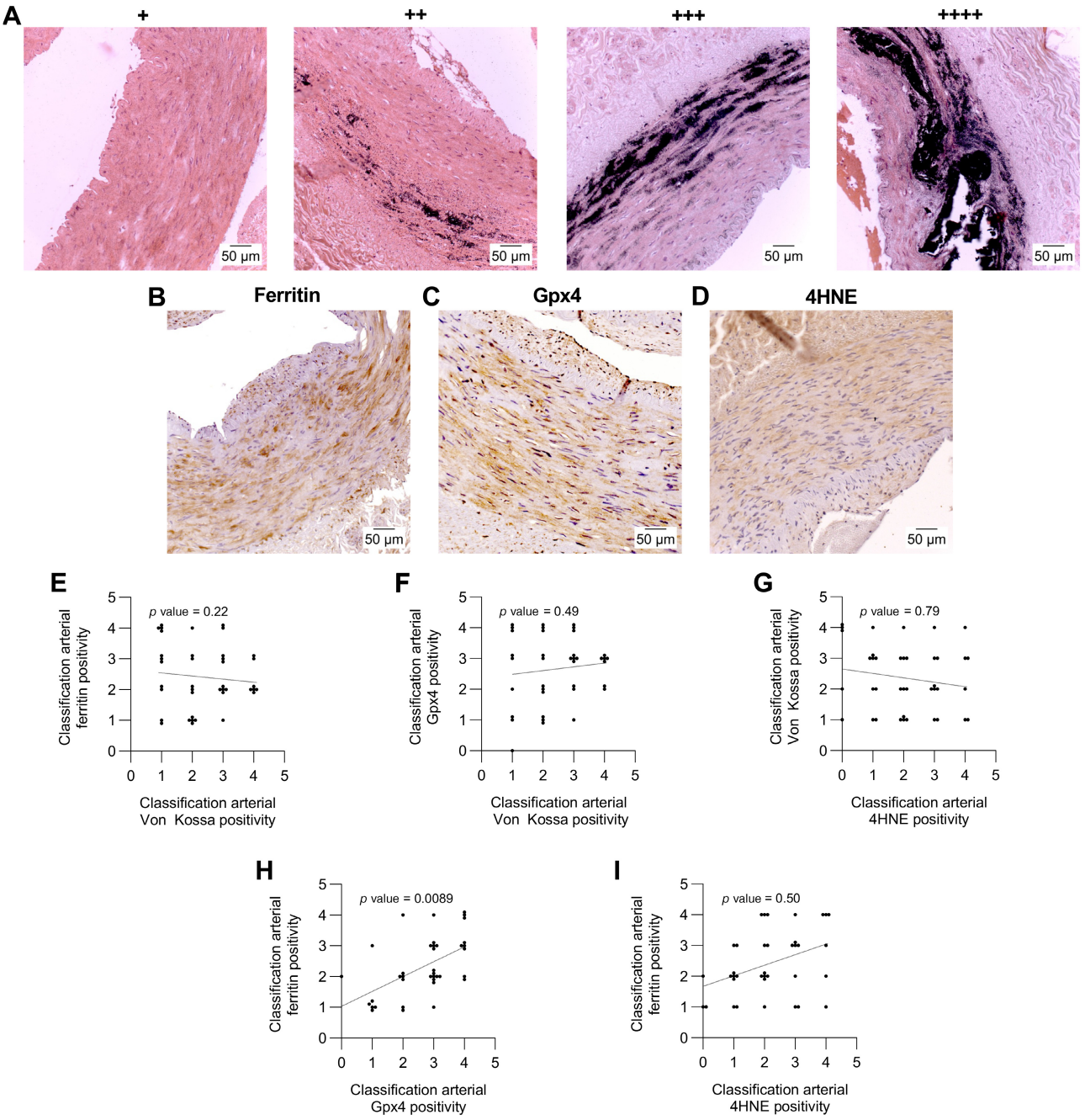

Figure 5. Assessment of staining patterns in human arterial tissue. (A) Human arterial tissue stained using Von Kossa's method illustrates different quantification categories. Signal intensity is classified as + = weak staining, ++ = mild staining, +++ = moderate staining and ++++ = strong staining. Images showing (B) ferritin, (C) Gpx4 and (D) 4HNE positivity. The association between Von Kossa classification and (E) ferritin expression, (F) Gpx4 expression and (G) the presence of 4HNE. The association between the presence of lipid peroxidation markers (H) Gpx4 and (I) 4HNE versus ferritin expression. Immunostained arterial sections were classified based on their signal intensities ranging from 0 = no staining to 4 = strong staining. 4HNE, 4-hydroxy-2-nonenal; Gpx4, glutathione peroxidase 4.

toxic lipid peroxides. The upregulation of Gpx4 could represent a protective mechanism to counteract elevated oxidative stress and lipid peroxidation. In this situation, the increase in the amount of Gpx4 might not be sufficient to fully counteract the wave of oxidative cellular stress. The presence of both Gpx4 and 4HNE in the calcified vessels of iron-treated CKD rats provides compelling evidence for a role of lipid peroxidation and possibly ferroptosis in the development of arterial calcification.

Moreover, ferritin/Gpx4/4HNE being present in calcified human arteries underlines the clinical relevance of our findings. The observation of clear ferritin expression in the human arteries implies accumulation of iron. The significant association between the expression of ferritin and Gpx4, which was also observed in iron-treated CKD rats, further substantiates this finding. This is particularly relevant as arterial iron accumulation correlates with both ferritin and Gpx4 expression in iron-treated CKD rats, and Gpx4 expression is a well known consequence of

intracellular iron-induced oxidative stress. The fact that no significant relationship was seen with 4HNE suggests that, in contrast to our observations in rats, the Gpx4-induced protective mechanism was sufficient to prevent excessive lipid peroxidation. This is also in line with the fact that iron accumulation in human tissue was not as pronounced as the iron accumulation seen in iron-treated CKD rats (no positive Turnbull staining). Thus, not surprisingly, arterial calcification was not associated with ferritin and Gpx4 expression/4HNE presence in human arteries.

In addition to arterial media calcification, patients with CKD often experience other cardiovascular diseases, including atherosclerosis. While the contribution of iron overload to arterial media calcification remains to be further elucidated, its potential causal role in atherosclerosis is also debated [48–50]. Although the rat model used in this study does not develop atherosclerosis, we observed several human arteries exhibiting signs of atherosclerosis (as evidenced by intimal fibrosis), which however did not show any association with the presence of iron (ferritin expression) in the arteries (results not shown).

Seemingly, i.v. iron treatment in the examined human cohort does not cause sufficient iron accumulation to be identified as a primary cause of arterial calcification. This observation aligns with the finding that the most pronounced effects of iron in the *in vivo* study were obtained after treatment with the highest iron dose (versus therapeutic dose). Furthermore, these results underscore the complexity of arterial calcification as a multifactorial disease wherein inducing factors like inflammation, uremic toxins, altered levels of calcification inhibitors (e.g. pyrophosphate and fetuin-A) and elevated serum phosphate levels may be of greater significance than iron accumulation. The findings of this study, however, recommend a careful approach to iron dosing in patients with CKD, tightly regulated with respect to the individual iron status of each patient.

The strengths of this study are linked to the inclusion of human arterial tissue alongside access to *in vivo* material, enhancing the relevance and applicability of the study findings. However, certain limitations need to be acknowledged. Alternative pathways underlying ferroptosis have not been further investigated, limiting the view of the broader scope of underlying mechanisms. Furthermore, access to human tissue was exclusively in the form of paraffin-embedded specimens, which leaves a gap in the variety of experiments that can be conducted, such as elemental calcium and iron analysis. Another limitation is the absence of an analysis of the effect of iron administration on arterial calcification in muscular arteries (e.g. femoral artery) next to elastic arteries (i.e. aorta in this study). Due to functional and morphological heterogeneity in the arterial tree, elastic and muscular arteries exhibit different susceptibilities to calcification [51]. Elastic arteries contain a relatively higher elastin content, making them more prone to elastin fragmentation [52]. These fractured elastic fibers form a nucleation scaffold for the deposition of calcium phosphate crystals and are involved in the induction of phenotypic switching of VSMCs [53,54]. However, despite these differences, previous publications from our team using the same adenine-induced CKD rat model demonstrated similar levels of calcification in both elastic and muscular arteries, suggesting a good correlation between both types of arterial tissue [55]. A fourth limitation is that we did not further delve into specific cell populations overlapping with the various signals. Given that arterial walls are composed of various cell populations next to VSMCs (e.g. macrophages and endothelial cells), investigating their individual role in this context could provide valuable insights [56,57].

In summary, i.v. iron treated CKD rats showed arterial iron sequestration, ferritin expression, lipid peroxidation and aggravated arterial calcification. Furthermore, arterial calcification correlated with arterial iron, ferritin and lipid peroxidation. Iron accumulated in the calcified arteries of patients receiving dialysis, which was accompanied by a lipid peroxidation/ferroptosis signature. However, the absence of a direct correlation with arterial calcification suggests that while iron loading may have contributed to the calcification process, it was not the predominant factor, highlighting the multifactorial nature of arterial calcification.

Acknowledgements

The authors gratefully acknowledge Hilde Geryl, Rita Marynissen, Axelle Belis, Geert Dams and Ludwig Lamberts for their excellent technical assistance. This study was funded by the Research Foundation Flanders (Fonds Wetenschappelijk Onderzoek, FWO) grant number G045120N, FWO scientific research network project W000321N and University Research Fund – Small Grant (Bijzonder Onderzoeksfonds UAntwerpen (BOF)/KP) 48542. AVdB, BO and SA are (postdoctoral) fellows of the FWO (1SD9222N, 12Z0422N and 1SH7Z24N).

Author contributions statement

AVdB conceptualized the research, carried out the experiment, analyzed the data and prepared the original draft. BO conceptualized the research and carried out the experiments. SA carried out the experiments. PE conceptualized the research and provided resources. TVB conceptualized the research and provided supervision and resources. AV conceptualized the research, provided supervision and resources and prepared the original draft. All authors revised the manuscript and agreed to the published version of the manuscript.

Data availability statement

The data underlying this article will be shared on reasonable request to the corresponding author.

References

1. Van den Branden A, Verhulst A, D'Haese PC, *et al*. New therapeutics targeting arterial media calcification: friend or foe for bone mineralization? *Metabolites* 2022; **12**: 327.
2. Cho IJ, Chang HJ, Park HB, *et al*. Aortic calcification is associated with arterial stiffening, left ventricular hypertrophy, and diastolic dysfunction in elderly male patients with hypertension. *J Hypertens* 2015; **33**: 1633–1641.
3. Sigrist MK, Taal MW, Bungay P, *et al*. Progressive vascular calcification over 2 years is associated with arterial stiffening and increased mortality in patients with stages 4 and 5 chronic kidney disease. *Clin J Am Soc Nephrol* 2007; **2**: 1241–1248.
4. Luengo-Fernandez R, Walli-Attaei M, Gray A, *et al*. Economic burden of cardiovascular diseases in the European Union: a population-based cost study. *Eur Heart J* 2023; **44**: 4752–4767.
5. Jankowski J, Floege J, Fliser D, *et al*. Cardiovascular disease in chronic kidney disease. *Circulation* 2021; **143**: 1157–1172.
6. Gafter-Gvili A, Schechter A, Rozen-Zvi B. Iron deficiency anemia in chronic kidney disease. *Acta Haematol* 2019; **142**: 44–50.
7. Macdougall IC, Bircher AJ, Eckardt KU, *et al*. Iron management in chronic kidney disease: conclusions from a "kidney disease: improving global outcomes" (KDIGO) controversies conference. *Kidney Int* 2016; **89**: 28–39.
8. Pigeon C, Ilyin G, Courselaud B, *et al*. A new mouse liver-specific gene, encoding a protein homologous to human antimicrobial peptide hepcidin, is overexpressed during iron overload. *J Biol Chem* 2001; **276**: 7811–7819.
9. Nicolas G, Bennoun M, Devaux I, *et al*. Lack of hepcidin gene expression and severe tissue iron overload in upstream stimulatory factor 2 (USF2) knockout mice. *Proc Natl Acad Sci U S A* 2001; **98**: 8780–8785.
10. Nemeth E, Tuttle MS, Powelson J, *et al*. Hepcidin regulates cellular iron efflux by binding to ferroportin and inducing its internalization. *Science* 2004; **306**: 2090–2093.
11. Ganz T. Molecular control of iron transport. *J Am Soc Nephrol* 2007; **18**: 394–400.
12. Nemeth E, Rivera S, Gabayan V, *et al*. IL-6 mediates hypoferremia of inflammation by inducing the synthesis of the iron regulatory hormone hepcidin. *J Clin Invest* 2004; **113**: 1271–1276.
13. Ganz T, Nemeth E. Iron balance and the role of hepcidin in chronic kidney disease. *Semin Nephrol* 2016; **36**: 87–93.
14. Jimenez K, Kulnigg-Dabsch S, Gasche C. Management of iron deficiency anemia. *Gastroenterol Hepatol (N Y)* 2015; **11**: 241–250.
15. Gutiérrez OM. Treatment of iron deficiency anemia in CKD and end-stage kidney disease. *Kidney Int Rep* 2021; **6**: 2261–2269.
16. Ramakrishnan L, Pedersen SL, Toe QK, *et al*. The hepcidin/ferroportin axis modulates proliferation of pulmonary artery smooth muscle cells. *Sci Rep* 2018; **8**: 12972.
17. Loick P, Mohammad GH, Cassimjee I, *et al*. Protective role for smooth muscle cell hepcidin in abdominal aortic aneurysm. *Arterioscler Thromb Vasc Biol* 2023; **43**: 713–725.
18. Sun MY, Zhang M, Chen SL, *et al*. The influence of hyperlipidemia on endothelial function of FPN1 Tek-cre mice and the intervention effect of tetramethylpyrazine. *Cell Physiol Biochem* 2018; **47**: 119–128.
19. Kawada S, Nagasawa Y, Kawabe M, *et al*. Iron-induced calcification in human aortic vascular smooth muscle cells through interleukin-24 (IL-24), with/without TNF-alpha. *Sci Rep* 2018; **8**: 658.
20. Koskenkorva-Frank TS, Weiss G, Koppenol WH, *et al*. The complex interplay of iron metabolism, reactive oxygen species, and reactive nitrogen species: insights into the potential of various iron therapies to induce oxidative and nitrosative stress. *Free Radic Biol Med* 2013; **65**: 1174–1194.
21. Huang M, Zheng L, Xu H, *et al*. Oxidative stress contributes to vascular calcification in patients with chronic kidney disease. *J Mol Cell Cardiol* 2020; **138**: 256–268.
22. Mody N, Parhami F, Sarafian TA, *et al*. Oxidative stress modulates osteoblastic differentiation of vascular and bone cells. *Free Radic Biol Med* 2001; **31**: 509–519.
23. Yang WS, Kim KJ, Gaschler MM, *et al*. Peroxidation of polyunsaturated fatty acids by lipoxygenases drives ferroptosis. *Proc Natl Acad Sci U S A* 2016; **113**: E4966–E4975.
24. Dixon SJ, Lemberg KM, Lamprecht MR, *et al*. Ferroptosis: an iron-dependent form of nonapoptotic cell death. *Cell* 2012; **149**: 1060–1072.
25. Veeckmans G, Van San E, Vanden BT. A guide to ferroptosis, the biological rust of cellular membranes. *FEBS J* 2023; **291**: 2767–2783.
26. Forcina GC, Dixon SJ. GPX4 at the crossroads of lipid homeostasis and ferroptosis. *Proteomics* 2019; **19**: 1800311.
27. Dalleau S, Baradat M, Guéraud F, *et al*. Cell death and diseases related to oxidative stress: 4-hydroxynonenal (HNE) in the balance. *Cell Death Differ* 2013; **20**: 1615–1630.
28. Shroff RC, McNair R, Figg N, *et al*. Dialysis accelerates medial vascular calcification in part by triggering smooth muscle cell apoptosis. *Circulation* 2008; **118**: 1748–1757.
29. Proudfoot D, Skepper JN, Hegyi L, *et al*. Apoptosis regulates human vascular calcification in vitro: evidence for initiation of vascular calcification by apoptotic bodies. *Circ Res* 2000; **87**: 1055–1062.
30. Wu X, Li Y, Zhang S, *et al*. Ferroptosis as a novel therapeutic target for cardiovascular disease. *Theranostics* 2021; **11**: 3052–3059.
31. Zhong S, Li L, Shen X, *et al*. An update on lipid oxidation and inflammation in cardiovascular diseases. *Free Radic Biol Med* 2019; **144**: 266–278.
32. Ma WQ, Sun XJ, Zhu Y, *et al*. Metformin attenuates hyperlipidaemia-associated vascular calcification through anti-ferroptotic effects. *Free Radic Biol Med* 2021; **165**: 229–242.
33. Ye Y, Chen A, Li L, *et al*. Repression of the antiporter SLC7A11/glutathione/glutathione peroxidase 4 axis drives ferroptosis of vascular smooth muscle cells to facilitate vascular calcification. *Kidney Int* 2022; **102**: 1259–1275.
34. Lu L, Ye Y, Chen Y, *et al*. Oxidized phospholipid POVPC contributes to vascular calcification by triggering ferroptosis of vascular smooth muscle cells. *FASEB J* 2024; **38**: e23592.
35. Hametner S, Wimmer I, Haider L, *et al*. Iron and neurodegeneration in the multiple sclerosis brain. *Ann Neurol* 2013; **74**: 848–861.
36. Kuragano T, Matsumura O, Matsuda A, *et al*. Association between hemoglobin variability, serum ferritin levels, and adverse events/mortality in maintenance hemodialysis patients. *Kidney Int* 2014; **86**: 845–854.
37. Bailie GR, Larkina M, Goodkin DA, *et al*. Data from the dialysis outcomes and practice patterns study validate an association between high intravenous iron doses and mortality. *Kidney Int* 2015; **87**: 162–168.
38. Kshirsagar AV, Freburger JK, Ellis AR, *et al*. Intravenous iron supplementation practices and short-term risk of cardiovascular events in hemodialysis patients. *PLoS One* 2013; **8**: e78930.
39. Song Y, Yang N, Si H, *et al*. Iron overload impairs renal function and is associated with vascular calcification in rat aorta. *Biometals* 2022; **35**: 1325–1339.
40. Seto T, Hamada C, Tomino Y. Suppressive effects of iron overloading on vascular calcification in uremic rats. *J Nephrol* 2014; **27**: 135–142.
41. Breborowicz A, Polubinska A, Górna K, *et al*. Iron sucrose induced morphological and functional changes in the rat kidney. *Transl Res* 2006; **148**: 257–262.
42. Zager RA, Johnson ACM, Hanson SY. Parenteral iron nephrotoxicity: potential mechanisms and consequences. *Kidney Int* 2004; **66**: 144–156.
43. Nuhu F, Seymour AM, Bhandari S. Impact of intravenous iron on oxidative stress and mitochondrial function in experimental chronic kidney disease. *Antioxidants (Basel)* 2019; **8**: 498.
44. Bulk M, Moursel LG, van der Graaf LM, *et al*. Cerebral amyloid angiopathy with vascular iron accumulation and calcification. *Stroke* 2018; **49**: 2081–2087.

45. Morvan M, Arangalage D, Franck G, *et al*. Relationship of iron deposition to calcium deposition in human aortic valve leaflets. *J Am Coll Cardiol* 2019; **73**: 1043–1054.
46. Agarwal R, Vasavada N, Sachs NG, *et al*. Oxidative stress and renal injury with intravenous iron in patients with chronic kidney disease. *Kidney Int* 2004; **65**: 2279–2289.
47. Mimić-Oka J, Savić-Radojević A, Pljesa-Ercegovac M, *et al*. Evaluation of oxidative stress after repeated intravenous iron supplementation. *Ren Fail* 2005; **27**: 345–351.
48. Guo Q, Qian C, Qian ZM. Iron metabolism and atherosclerosis. *Trends Endocrinol Metab* 2023; **34**: 404–413.
49. Cornelissen A, Guo L, Sakamoto A, *et al*. New insights into the role of iron in inflammation and atherosclerosis. *EBioMedicine* 2019; **47**: 598–606.
50. Vinchi F, Porto G, Simmelbauer A, *et al*. Atherosclerosis is aggravated by iron overload and ameliorated by dietary and pharmacological iron restriction. *Eur Heart J* 2020; **41**: 2681–2695.
51. Schlieper G. Vascular calcification in chronic kidney disease: not all arteries are created equal. *Kidney Int* 2014; **85**: 501–503.
52. Leloup AJA, Van Hove CE, Heykers A, *et al*. Elastic and muscular arteries differ in structure, basal NO production and voltage-gated Ca(2+)−channels. *Front Physiol* 2015; **6**: 375.
53. Persy V, D'Haese P. Vascular calcification and bone disease: the calcification paradox. *Trends Mol Med* 2009; **15**: 405–416.
54. Simionescu A, Philips K, Vyavahare N. Elastin-derived peptides and TGF-beta1 induce osteogenic responses in smooth muscle cells. *Biochem Biophys Res Commun* 2005; **334**: 524–532.
55. Opdebeeck B, Maudsley S, Azmi A, *et al*. Indoxyl sulfate and *p*-cresyl sulfate promote vascular calcification and associate with glucose intolerance. *J Am Soc Nephrol* 2019; **30**: 751–766.
56. Li D, Fan C, Li X, *et al*. The role of macrophage polarization in vascular calcification. *Biochem Biophys Res Commun* 2024; **710**: 149863.
57. Zhao L, Yang N, Song Y, *et al*. Effect of iron overload on endothelial cell calcification and its mechanism. *Ann Transl Med* 2021; **9**: 1658.

SUPPLEMENTARY MATERIAL ONLINE

Figure S1. Images of stained arterial tissue of non-CKD rats treated with vehicle, 3 or 10 mg/kg iron stained for (A) iron, (B) ferritin, (C) Von Kossa, (D) Gpx4 and (E) 4HNE. 4HNE, 4-hydroxy-2-nonenal; CKD, chronic kidney disease; Gpx4, glutathione peroxidase 4

Figure S2. Von Kossa (upper panel) and Alizarin red staining (lower panel) show (A) equal patterns of calcification in calcified aortas of CKD rats and (B) no staining in non-CKD animals. (C) As indicated by the arrows, smaller calcified spots could only be detected by Von Kossa staining, not by Alizarin red staining. CKD, chronic kidney disease

Figure S3. Overview of representative images of human arterial tissue stained for (A) ferritin, (B) Gpx4 and (C) 4HNE and each category (+, ++, +++ and ++++). 4HNE, 4-hydroxy-2-nonenal; Gpx4, glutathione peroxidase 4

Figure S4. Classification of human arterial tissue stained for Von Kossa, ferritin, Gpx4 and 4HNE performed by the second observer